Bond behaviour of light and heavy carbon fibre TRM to masonry interfaces

Kuanysh T. Makashev[a], Savvas P. Triantafyllou[b,*], Georgia E. Thermou[c], Walid Tizani[c]

[a] *Faculty of Engineering, Toraighyrov University*
Lomov Street, 64,Pavlodar,140008,Kazakhstan
[b] *Institute for Structural Analysis and Aseismic Research, School of Civil Engineering*
National Technical University of Athens, Zografou Campus, Greece
[c] *Centre for Structural Engineering and Informatics, Faculty of Engineering*
The University of Nottingham, NG2 2RD, UK

Abstract

We present the results of an experimental campaign on the bond behaviour between carbon fibre textile reinforced mortars and masonry substrate. The campaign involved 54 single lap direct shear tests on masonry wallettes reinforced with a single TRM layer. The key investigated parameters were the type of the textile fibre material (light carbon and heavy carbon), the coating of the textile reinforcement with epoxy resin, and the bond length (100, 150, 200, and 250 mm). The results highlight the beneficial effect of the epoxy resin coating that practically doubles the maximum attained loads. This increase is shown to be associated to a consistent shift of the failure mode from textile slippage to detachment at the matrix to matrix interface. In the uncoated specimens, the maximum load is practically identical for heavy and light carbon. Conversely, in the coated specimens the maximum load attained by the heavy carbon fibre textiles is 65% higher than that of the light carbon coated fibre textiles. However, both coated textiles demonstrate the same exploitation ratio. Cost-wise, this renders light carbon an appealing choice in practical applications. The experimental observations are further examined in view of analytical modelling.

Keywords: carbon fibre textile, TRM, masonry, bond, strengthening

1. Introduction

Unreinforced masonry structures (URM) constitute a significant portion of the global building stock [1]; most notably, they involve structures of extreme cultural and historical importance. Interventions in the form of structural strengthening are necessary to mitigate the adverse effects of ageing and also increase their bearing capacity vis-à-vis natural and man-made hazards [2].

Over the past years, a large number of techniques has been proposed for the strengthening of URM structures, e.g., surface treatment, shotcrete or ferrocement overlays, Fibre Reinforced Polymers (FRP), Textile Reinforced Mortars (TRM), and grout or epoxy resin injections [1, 3]. FRP and TRM in particular have emerged as highly efficient and low footprint strengthening solutions; they both harness the advantages of high strength composites.

TRM, also referred to in the literature as Fibre Reinforced Cementitious Matrices (FRCM), involve high strength textile fibre materials embedded in inorganic cement based mortars. Currently, a variety of different fibre textiles is available in the market, e.g., glass, carbon, basalt, aramid, polypropylene (PP), polyparaphenyle benzobisoxazole (PBO), or steel textiles [4]. Research

*Institute for Structural Analysis and Aseismic Research, School of Civil Engineering, National Technical University of Athens, Zografou Campus, Athens 15780, Greece, e-mail: savtri@mail.ntua.gr

conducted over the past 15 years has clearly highlighted the efficiency of TRM for the strengthening of masonry structures [5–10].

A key parameter in the effectiveness of TRM is the bond between the composite material and the masonry substrate. This interfacial property has been found to often be the weak link in TRM strenthening resulting in under-utilisation of the textile fibre material, which is the expensive constituent of the composite material [10]. According to the RILEM reccomendations [11], six failure modes are typically identified as shown in Fig. 1, i.e., (A) cohesive debonding in the masonry; (B) debonding at the matrix-to-substrate; (C) debonding at the textile-to-matrix interface; (D) sliding of the textile within the matrix, and (E1) partial or (E2) complete tensile rupture of one or more fibre yarns, respectively.

To this point, a significant number of experimental and analytical studies has been performed to investigate the mechanisms governing the TRM to masonry bond behaviour for varying bond lengths and also different textile fibre materials, i.e., glass (see, e.g, [12]), carbon [13] and steel fibre textiles [14]. Driven by experiments performed in polymer based composites, two test setups have been utilised for this purpose, i.e., single-lap, see., e.g., [12, 15, 16] - and double-lap shear tests [4, 13, 17]. In [18] a thorough comparison on the the two test setups was performed showing that they both provide consistent results vis-à-vis the maximum loads and the corresponding failure modes.

A double-lap test setup was utilized in [19] to test carbon fibre TRMs considering three bond lengths, i.e., 110mm, 230mm, and 350mm concluding on an effective bond length lower than 110mm. In Ref. [20], the authors performed a series of double lap tests on TRMs with varying textile fibre materials and demonstrated that the latter significantly affect the bond failure mode. The typical failure mode of the carbon fibre textiles in this case was textile slippage. Conversely, a series of tests conducted in [21] on carbon fibre textiles with a different mesh size highlighted the textile to matrix interface as a typical failure mode.

The mortar properties, i.e., its thickness, stiffness, and tensile strength have also been shown to impact on the initial stiffness and cracking stress of the bond [22]. Reference [23] further confirmed that the mortar mix significantly affects the TRM to masonry bond. Very recently, the bond performance under high temperature has also been investigated [24, 25] highlighting the advantages of TRM systems when compared to FRP.

Despite the considerable amount of experimental research conducted in the field, results are characterized by a significant scatter, largely due to the uncertainties pertinent to the constituent materials involved and also the large variety of textile fibre configurations available in the market. This brings forward the requirement for further experimental testing to identify the key parameters affecting the TRM to masonry bond and quantify their influence. In this work, we performed a total of 54 single lap shear bond tests considering 16 different TRM configurations. The key investigated parameters of this experimental campaign were the textile fibre material (light carbon and heavy carbon), the in-house epoxy coating applied on the textile and the bond length (100, 150, 200, and 250 mm). To the authors' knowledge, this is the first time this set of parameters is considered within a single experimental campaign.

The rest of the paper is organised as follows. The properties of the materials used, the experimental configurations, and the specimen typologies employed in this experimental campaign are presented in Section 2. The single lap direct shear test experimental results are presented and discussed in Sections 3 and 4, respectively. Our concluding remarks are provided in Section 6.

2. Experimental program

2.1. Specimens and investigated parameters

The main purpose of this experimental campaign was to investigate the bond mechanisms involved in masonry coupons strengthened with textile reinforced mortars. The key investigated parameters were: (a) the textile fibre material (light and heavy carbon textiles) (b) the bond length L_b

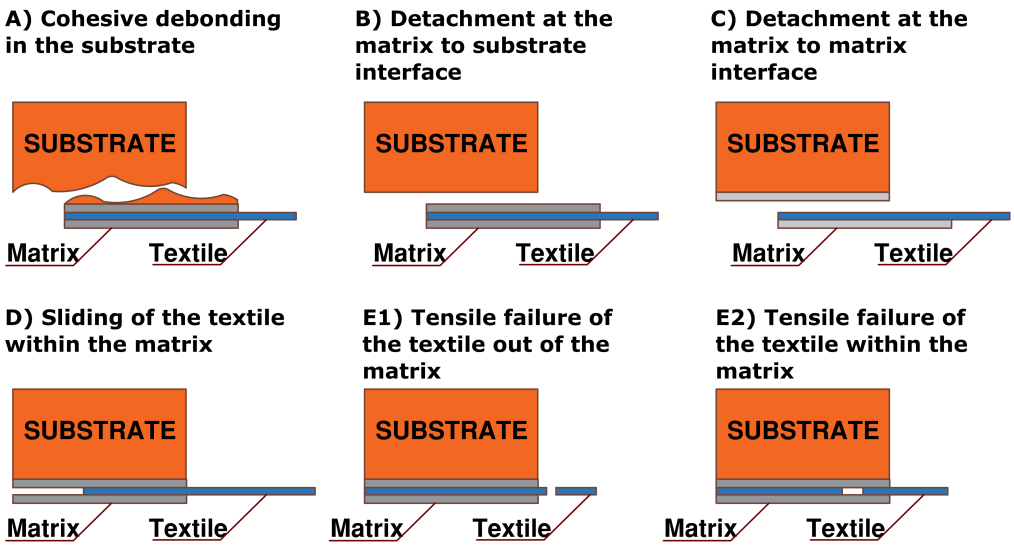

Figure 1: Failure modes

(100, 150, 200, and 250mm), and (c) the epoxy resin coating.

In total 54 specimens, with overall dimensions of 365 x 215 x 102.5 mm (Fig. 2), were prepared and tested. Each masonry wallette comprised 5 bricks irrespective of the bond length.

The walletes were strengthened with a single TRM layer, one week after construction. The width of the textile was $b_f = 120$ mm in all cases. The dry textile length was L_f =400 mm in all cases as shown in Fig. 2a. All specimens were tested one month after construction. The application of the TRM layer was performed according to the following procedure:

(a) Air pressure was used to remove dust from the masonry wall surface;
(b) The wall was slightly dampened and a first layer of mortar was applied at the entire surface of the wall Fig. 3a;
(c) The textile layer was applied and impregnated into the previously applied mortar using hand pressure Fig. 3b;
(d) A final layer of mortar was applied to completely cover the textile Fig. 3c. The total thickness of the TRM was targeted at 6 mm, similar to the bond tests conducted in [26].

In our previous works [27–29] we found that a 6-7 mm TRM layer thickness is an easy to achieve, easy to work with and and well-behaved value.

It is of interest to note that the the application of the TRM layer was performed with the wallette positioned vertically to better emulate the actual, on site, application practice. Hence, the TRM layer thickness was not a controlled but rather a targeted parameter. Measurements of the thickness prior to testing showed that the targeted value of 6mm was achieved within a 5% margin.

The procedure was completed while the mortar was fresh to achieve optimum adhesion of the TRM layer. The final strengthened configuration is shown in Fig. 3c. An unbonded margin of 25 mm was considered in all specimens, Fig. 2a, to minimise the impact of edge effects, i.e., avoid stress concentrations [11, 30].

The specimens with their corresponding parameters are shown in Table 1. The naming convention adopted is X_Y, where X corresponds to the textile fibre material (Ch-heavy carbon, Cl-light carbon) and Y corresponds to the bonded length. The suffix 'co' is appended when the textile fibre material has been coated with epoxy resin. The total number of TRM configurations tested was 16. Three specimens per configuration were tested; a fourth one was tested only when the coefficient of variation exceeded a threshold

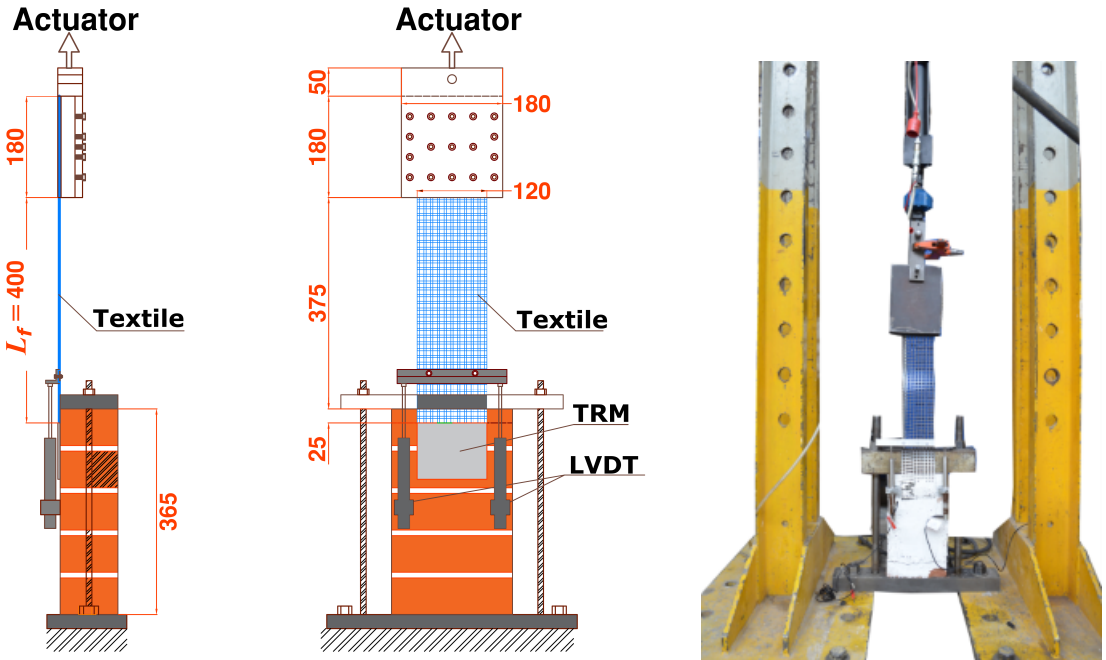

(a) (b)

Figure 2: Test setup (a) test setup details (all dimensions in mm), (b) actual test setup

(a) (b) (c)

Figure 3: TRM layer application steps.

value of 10%. The total number of specimens per configuration is also shown in Table 1.

2.2. Materials

Typical clay bricks, available in the UK market, were used with nominal dimensions of 215 x 102.5 x 65 mm. A 1:4 cement to sand ratio was used for the joint mortar mix. The amount of water was defined through trial mixes, until the desired workability was achieved. The brick compressive strength was determined according to BS EN 772-1 [31]. Five bricks were tested and the compressive strength was found equal to 19.85 MPa with a CoV of 15%.

The inorganic mortar used for the TRM matrix was a dry binder comprising cement and polymers at a ratio 8:1 by weight. The water to mortar ratio was 0.23 by weight.

The tensile and compressive strength for the joint and strengthening mortars were determined via prism tests according to the EN 1015-11 [32]. Nine prisms were tested in three point bending to determine the tensile strength. The ruptured segments were used to define the uniaxial compressive strength on a bear surface of 40x40 mm. The tensile and compressive strengths for all mortars are shown in Table 2.

Two different carbon fiber textiles were used in this study, i.e., light carbon with a surface density equal to 220 g/m^2 and heavy carbon with a surface density equal to 348 g/m^2. Both textiles consisted of uncoated carbon fibers; these were equally distributed in two orthogonal directions. The difference in the weight per unit area resulted in a different equivalent thickness between the two textiles. This is reported in Table 3. The weaving pattern of the two textiles was very similar. In both cases, the fiber rovings in two orthogonal directions were simply stitched together with the aid of polypropylene fibers.

The mesh sizes and the mechanical properties of the textile fibres, according to the manufacturer data sheets, are shown in Table 3. The geometric layout of the two textiles is schematically shown in Fig. 2.2 where the width, the area (A_{rov}), and the thickness (t_{rov}) of each individual roving are shown. The TEX value of each textile which measures the linear density is also provided.

In the coated specimens, coating was performed in-house using an epoxy resin with a 2:1 mix ratio by weight. According to the corresponding datasheet, the elastic modulus and tensile strength of the epoxy resin was 1.8 GPa and 37 MPa, respectively. The coating of the textile fibre material was performed according to the following procedure:

(i) The textile was cut in strips with nominal dimensions W =120 mm and L =1000 mm;
(ii) the textile was placed flat onto a work-bench, taped to prevent slip and painted using a roller with a foam nozzle;
(iii) the coated textile was left on the table for 2 days to allow the resin to cure before being used for TRM strengthening.

It is essential to note that in all cases the mesh size and the corresponding application procedure ensured that the roving spacings were not filled/ covered by resin.

2.3. Textile fibre material coupon tests

The mechanical properties of the four types of textile fibre materials used in this study, i.e., light carbon, coated light carbon, heavy carbon, and coated heavy carbon were characterised via tensile testing as per the ASTM D5034 [33] specifications. In all cases, the free length of the specimen was 250 mm and the width was 80 mm. Three identical specimens were tested per case to reduce the variability. All samples were cut in the wrap direction of the textile rolls.

The tests were performed using displacement control at a rate of 0.02 mm/sec in a Zwick universal testing machine fitted with a 200kN load cell. The loading rate was chosen to ensure quasi-static loading conditions. The elongation was measured using two LVDTs with a 15 mm stroke and a 0.01 mm sensitivity (Fig. 5).

The failure mode in all specimens was textile rupture in the central region as shown in Fig. 6. The corresponding stress strain curves are shown in Fig. 7. The tensile stress was calculated by

Table 1: Specimen configurations and naming convention

Specimen	**Bond Length [mm]**	**Samples**	**Textile fibre**	**Coating**
Cl_100	100	3	Light carbon	No
Cl_150	150	4	Light carbon	No
Cl_200	200	4	Light carbon	No
Cl_250	250	3	Light carbon	No
Cl_100_(co)	100	4	Light carbon	Yes
Cl_150_(co)	150	3	Light carbon	Yes
Cl_200_(co)	200	3	Light carbon	Yes
Cl_250_(co)	250	3	Light carbon	Yes
Ch_100	100	3	Heavy carbon	No
Ch_150	150	4	Heavy carbon	No
Ch_200	200	4	Heavy carbon	No
Ch_250	250	3	Heavy carbon	No
Ch_100_(co)	100	3	Heavy carbon	Yes
Ch_150_(co)	150	3	Heavy carbon	Yes
Ch_200_(co)	200	3	Heavy carbon	Yes
Ch_250_(co)	250	4	Heavy carbon	Yes

Table 2: Mortar properties

Mortar	**Tensile strength [MPa]**	**Compressive strength [MPa]**
Joint mortar	1.85 (0.50*/0.26**)	7.82 (0.36*/0.04**)
Strengthening mortar (W/M=0.23)	4.95 (0.17*/0.03**)	28.90 (0.17*/0.02**)

*Standard deviation/ **Coefficient of Variation

Table 3: Textile fibre material parameters.

	Heavy carbon	Light Carbon
Weight [g/m^2]	348	220
Density [g/cm^3]	1.8	1.8
Nominal thickness [mm]	0.097	0.062
Tensile strength* [MPa]	3800	4800
Young's modulus* [GPa]	225	225

* as reported in the manufacturers' datasheets

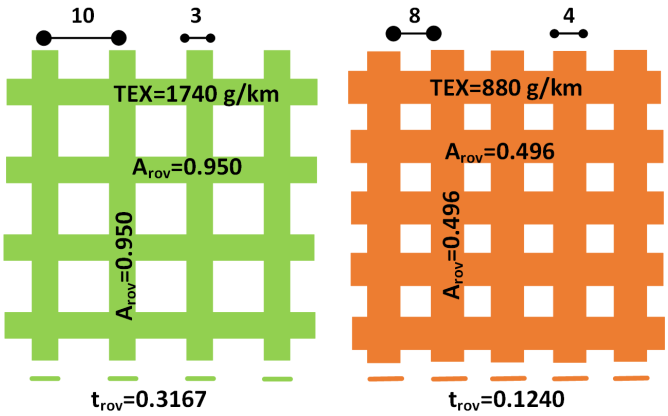

(a) (b)

Figure 4: Geometry layout of carbon fibre textiles (a) heavy carbon and (b) light carbon. Dimensions are in mm unless otherwise stated.

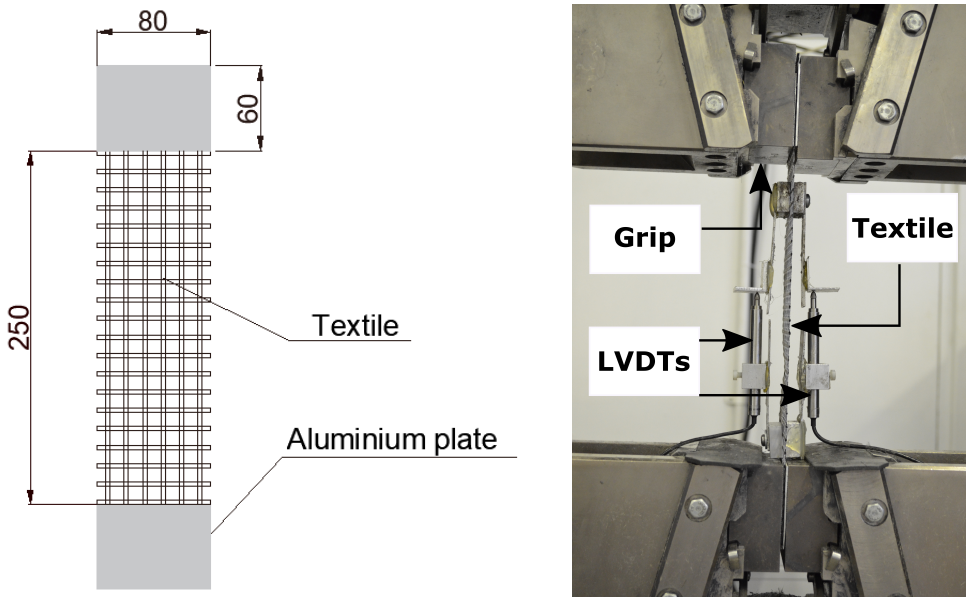

(a) (b)

Figure 5: Test setup (a) Geometry of textile coupon (all dimensions are in mm), (b) Actual test setup

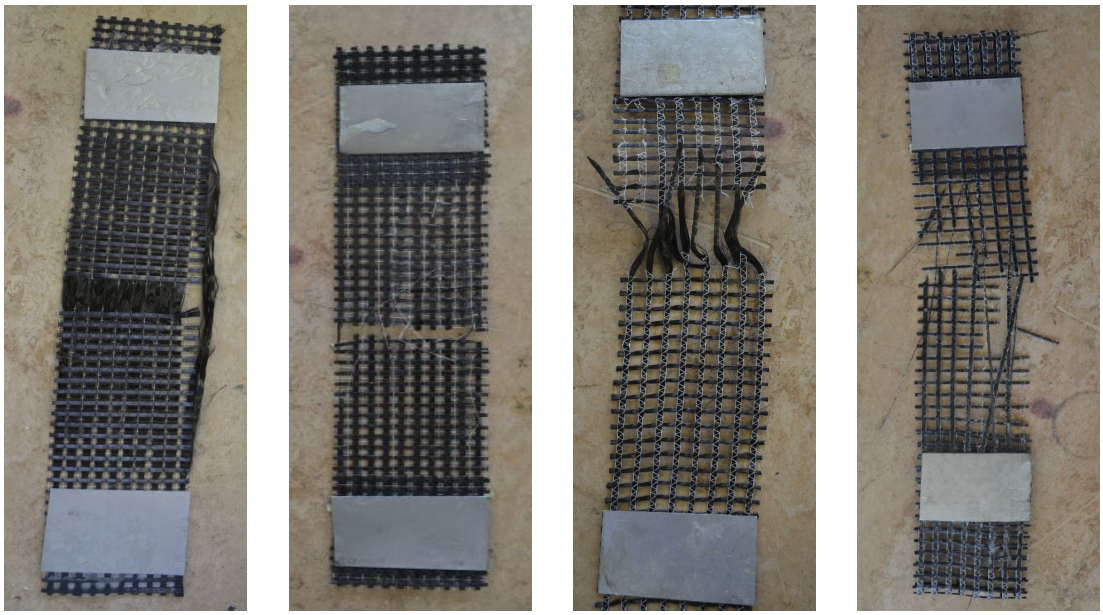

(a) (b) (c) (d)

Figure 6: Fibre textile tensile tests failure modes. All specimens failed by textile rupture: (a) light carbon; (b) light carbon coated; (c) heavy carbon; (d) heavy carbon coated.

dividing the applied load to the textile cross sectional area; the latter corresponds to the coupon width multiplied by the nominal thickness shown in Table 3. The resulting mean values of the fibre textile peak strength f_f^u, the corresponding strain ε_f^u, and the modulus of elasticity E_f are shown in Table 4. The measured values on the uncoated textiles are practically half the manufacturer values shown in Table 3. This was anticipated as the latter refer to the tensile strength of a single fibre. The results obtained in the present study agree well with the results reported in [34] on the same textile meshes and using the same test specifications.

2.4. Single lap direct shear test setup

The walletes were clamped to the strong floor using a steel reaction frame as shown in Fig. 2. The steel frame comprised two steel plates connected with four threaded stainless steel rods. The textile fibre material was attached to the actuator through steel plates; these were connected together via a set of seventeen bolts. Rubber plates were installed at the plate/ textile interface to increase friction and prevent damage to the textile. All bolts were fastened using a torque wrench.

Two LVDTs with a 20 mm stroke and a 0.05 mm sensitivity were used to measure relative displacements between the TRM and the brick substrate. Displacements were also captured with Digital Image Correlation (DIC), see, also, Fig. 8; the TRM surface was painted white to facilitate DIC measurements.

The load was applied using a servo-hydraulic actuator fitted with a load cell with a maximum capacity of 100 KN at a displacement rate of 0.003 mm/s, i.e., 0.18 mm/ min which is typical for TRM to masonry bond tests [see, e.g., 35] and ensures quasi-static conditions. Data was collected, synchronised and recorded using a fully-computerised data acquisition system at a frequency of 4 Hz.

3. Bond test experimental results

3.1. Force - slip response

The force-slip paths for all specimens are shown in Fig. 9. The slip shown in the plots is the average value of the LVDT measurements. These matched the measurements retrieved from DIC post-processing with minor deviations. For each group of identical specimens, the force-slip paths were derived by averaging the results of the three

Table 4: Tensile test results on fibre-textile materials

Textile	f_f^u [MPa]	ε_f^u [%]	E_f [GPa]
Carbon (light)	1295 (205)* (0.15)**	0.90 (0.12)* (0.14)**	140 (5.68)* (0.08)**
Carbon (light) coated	2368 (117)* (0.04)**	1.27 (0.11)* (0.09)**	170 (10)* (0.06)**
Carbon (heavy)	1258 (103)* (0.08)**	0.73 (0.05)* (0.07)**	160 (17)* (0.10)**
Carbon (heavy) coated	2541 (347)* (0.13)**	1.20 (0.30)* (0.25)**	196 (9.5)* (0.06)**

*Standard deviation, **Coefficient of variation

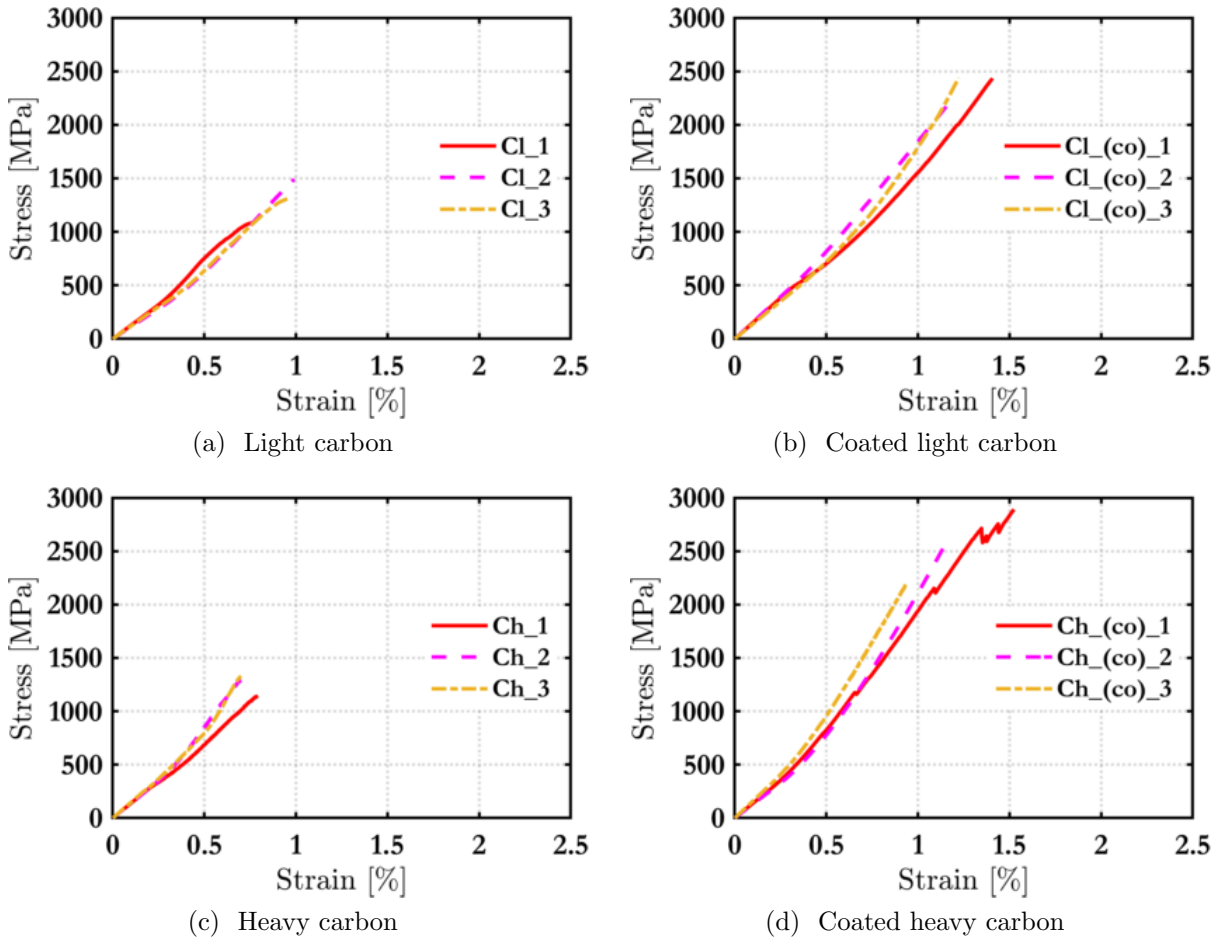

(a) Light carbon

(b) Coated light carbon

(c) Heavy carbon

(d) Coated heavy carbon

Figure 7: Fibre textile tensile tests: Stress strain curves

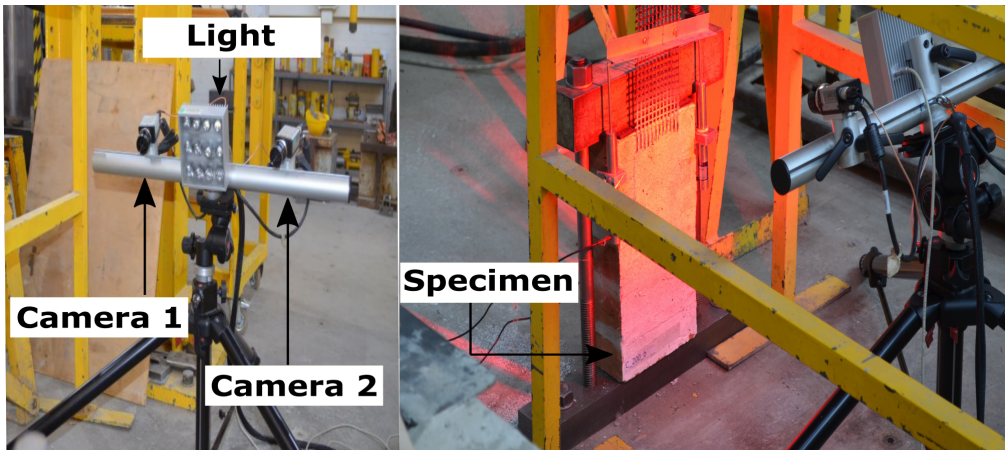

Figure 8: Test setup

specimens that resulted in the lowest coefficient of variation; the failure mode was examined and found identical for each group.

The force-slip paths shown in Figs. 9a and 9c for the uncoated light and heavy carbon specimens, respectively demonstrate a linear increasing branch up to a maximum load followed by a gradual reduction until the experiment is stopped. However, the response of the the coated light and heavy carbon specimens, shown in Figs. 9b and 9d, respectively are characterized by a sudden drop after the maximum load.

The maximum loads P_{max}, the maximum stresses at the textile f^b_{max}, and the corresponding failure modes are summarized in Table 5 for all specimens. The maximum stress was evaluated as

$$f^b_{max} = \frac{P_{max}}{t_f \cdot b_f}, \tag{1}$$

where t_f is the nominal thickness of the textile shown in Table 3 and $b_f = 120$ mm the width of the textile. In deploying the nominal thickness to evaluate the stress, the contribution of the rovings vertical to the loading direction is neglected in the stress transfer mechanism. However, we opt for this stress measure to be consistent with the literature, noting also that the wrap and weft yarns in the examined textiles are identical.

In terms of maximum load, the highest value was recorded for the case of coated heavy carbon Ch_250_(Co) at a bond length of 250mm ($P_{max} =$ 16.11 kN). The lowest value was recorded in the case of Cl_100 and Ch_100 and was approximately 5.5 kN. In terms of slip at P_{max}, the lowest value was recorded in the uncoated heavy carbon specimen Ch_250 and was equal to 0.9mm. The highest value was recorded for the case of the Ch_250_(Co) specimen and was equal to 1.7mm.

3.2. Failure modes

The failure modes observed for the different bond lengths are shown in Figs. 10 and 11 for the light carbon, and heavy carbon textile fibre specimens, respectively. All non coated specimens failed due to textile slippage. The corresponding force-slip paths shown in Fig. 9a and 9c for the light carbon and heavy carbon specimens respectively demonstrate a residual strength that is consistent with the observed failure mode. Conversely, all coated specimens failed with detachment at the matrix to matrix interface. In this case, failure was abrupt as manifested in the corresponding force-slip paths for the light (Fig. 9b) and the heavy (Fig. 9d) coated carbon specimens, respectively.

4. Discussion

4.1. The effect of the bond length

The variation of the average P_{max} in all materials for increasing values of the bond length is shown in Fig. 12. In all cases, the trend is practically bilinear, with the exception of the coated heavy carbon fibre textile strengthened specimens.

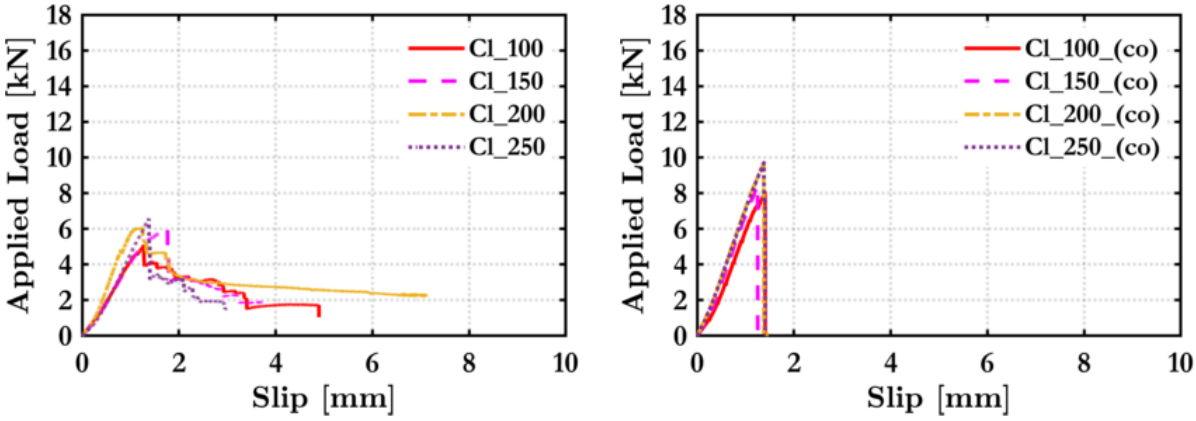

(a) Light carbon

(b) Coated light carbon

(c) Heavy carbon

(d) Coated heavy carbon

Figure 9: Experimental bond tests results

Table 5: Bond test results

Specimen	Maximum Load P_{max}			Maximum Stress f^b_{max}			Failure mode
-	Mean [kN]	St. deviation [kN]	CoV -	Mean [MPa]	St. deviation [MPa]	CoV -	
Cl_100	5.44	0.33	0.08	731	55	0.08	D
Cl_150	6.07	0.20	0.03	815	27	0.03	D
Cl_200	6.32	0.23	0.04	849	30	0.04	D
Cl_250	6.57	0.47	0.07	883	63	0.07	D
Cl_100_(co)	8.04	0.66	0.08	1080	89	0.08	C
Cl_150_(co)	8.44	0.16	0.02	1133	21	0.02	C
Cl_200_(co)	9.61	0.83	0.09	1292	112	0.09	C
Cl_250_(co)	9.71	0.38	0.04	1304	51	0.04	C
Ch_100	5.53	0.72	0.13	475	62	0.13	D
Ch_150	6.01	0.74	0.01	548	8	0.01	D
Ch_200	6.60	0.54	0.08	567	46	0.08	D
Ch_250	6.65	0.51	0.08	571	44	0.08	D
Ch_100_(co)	10.73	0.71	0.07	922	61	0.07	C
Ch_150_(co)	10.77	0.59	0.05	925	51	0.05	C
Ch_200_(co)	15.06	1.03	0.07	1293	89	0.07	C
Ch_250_(co)	16.11	0.59	0.04	1384	50	0.04	C

(a) 100mm (b) 150mm (c) 200mm (d) 250mm

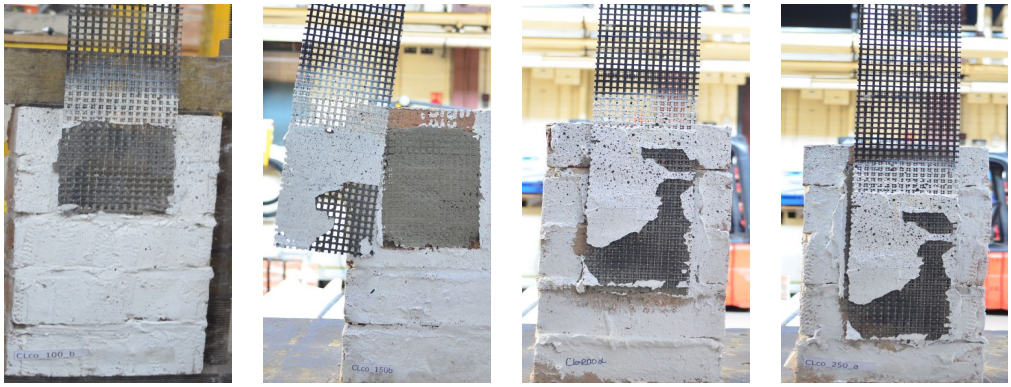

(e) 100mm (f) 150mm (g) 200mm (h) 250mm

Figure 10: Typical failure modes of specimens strengthened with light carbon textile: (a)-(d) uncoated specimens, failure mode: Textile slippage; (e)-(h) coated specimens, failure mode: detachment.

(a) 100mm (b) 150mm (c) 200mm (d) 250mm

(e) 100mm (f) 150mm (g) 200mm (h) 250mm

Figure 11: Typical failure modes of specimens strengthened with heavy carbon textile: (a)-(d) uncoated specimens, failure mode: Textile slippage; (e)-(h) coated specimens, failure mode: detachment.

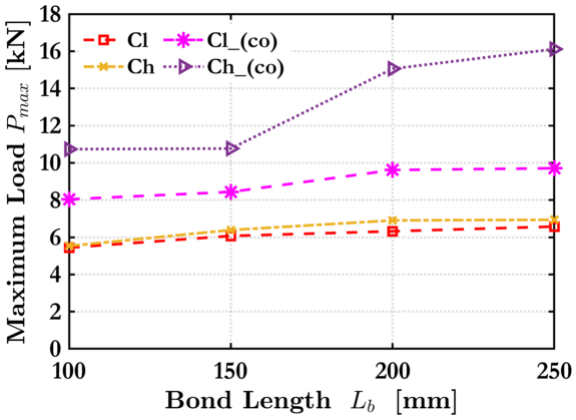

Figure 12: Variation of the maximum load as a function of the bond length

Increasing values of the bond length resulted in increasing values of the maximum attained load P_{max}. With the exception of the coated heavy carbon textile fibre specimens, after a certain bond length the maximum load tends to stabilise (Fig. 12); this bond length corresponds to the effective bond length, L_{eff}. The effective bond length is in the range of 200-250 mm for the uncoated heavy and light and the coated light carbon specimens.

The effective bond length seems to be larger than 250 mm for the case of the heavy coated carbon textile fibre specimens where failure was manifested by detachment at the matrix to matrix interface. This is indicative of the fact that the strengthening mortar employed in this experimental campaign would not enable the textile to develop its tensile strength.

4.2. The effect of the textile fibre material and in house coating

We consider here the average values of P_{max} for the case of L_b=250 mm as reported in Table 5. The uncoated light and heavy textile fibre specimens practically attained the same maximum load; this agrees with the observed failure mode, i.e., textile slippage in both cases. Hence, the textile to matrix interface properties seem to largely depend on the smoothness of the roving surface rather than the geometry of the textile mesh.We further note that the entire contact surface in both cases is comparable. Excluding the edge yarns, the heavy textile fibre material has roughly a contact surface equal to (31 yarns x 0.95) 29.5 mm^2 in both directions. The corresponding value for the light textile fibre material is (56 x 0.496) 27.7 mm^2.

The exploitation ratio is defined according to Eq. (2) as

$$\rho_{TRM} = f^b_{max}/f^u_f, \tag{2}$$

where we note that for all cases the tensile strength of the corresponding uncoated textile is employed in the denominator. This is to better highlight the influence of coating on the mechanical performance of the composite system. The exploitation ratios are plotted versus the bond length for each textile fibre material in Fig. 13.

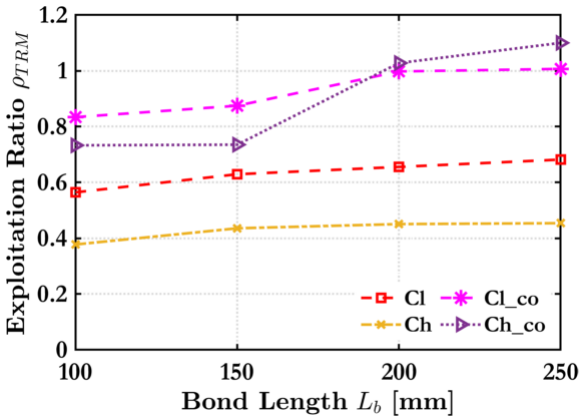

Figure 13: Exploitation ratio vs bond length

Since the light carbon fibre textile has a lower nominal thickness (Table 3), a 1.5 times higher exploitation ratio is achieved in the case of the light carbon textile fibre material as shown in Fig. 13.

All coated specimens demonstrated increased values of P_{max} compared to the corresponding uncoated ones. In particular, the maximum load recorded for the 250 mm coated heavy carbon specimen increased by 142% compared to the uncoated one. The corresponding increase for the 250mm coated light carbon fibre textile was 48%. Since the failure mode was identical for the coated heavy and coated light carbon specimens, i.e., detachment at the textile to fibre interface, the different effect the coating rendered on P_{max} is attributed to the coarser mesh of the heavy carbon textile; this allows for for an unhindered penetra-

tion of the mortar through the textile, thus enhancing the interlocking mechanism. However, it is of interest to note that the coated light and heavy carbon fibre textiles demonstrate practically identical exploitation ratios as shown in Fig. 13 hence rendering the light carbon fibre textile a more viable strengthening solution due to its lower cost.

The beneficial effect of coating is two-fold. On the one hand, it increases the rigidity of the flexible mesh hence facilitating its application. In addition, it enhances the fibre to matrix stress transfer mechanism by bonding the inner and outer filaments of the rovings, also increasing the surface roughness of the latter. As a result, the distribution of stresses in the textile becomes more uniform and the fibres are better utilised in carrying tensile forces. This is further reflected in Fig. 13 where all coated specimens demonstrate increased exploitation ratios compared to their uncoated counterparts. This becomes particularly evident when observing the failure modes of the specimens, which shifted from textile slippage to detachment at the matrix to matrix interface.

To investigate this hypothesis, P_{max} is plotted against the axial stiffness of the textile for the uncoated and the coated specimens in Figs. 14a and 14b, respectively. In each figure, 4 lines are plotted each corresponding to a particular bond length. The axial stiffness of the each textile is evaluated as $K_t = t_f \cdot E_f$, where t_f is the nominal thickness shown in Table 3 and E_f is the Young's modulus determined from the tensile tests as shown in Table 4.

In the uncoated specimens, the effect of the axial stiffness is practically negligible. Furthermore, the spread between the lines corresponding to the different bond lengths is marginal. This clearly agrees well with the observed failure mode, i.e., textile slippage; the interface mechanism between the textile and the mortar dictates the response.

Conversely, in the case of the coated specimens (Fig. 14b), the increased axial stiffness is shown to magnify the effect of the bond length on P_{max} as manifested by the distance between the lines corresponding to identical bonded lengths. This further highlights the beneficial effect of the textile stiffness on enabling the uniform distribution of stresses within the matrix. Furthermore, for the same L_b, the maximum load increases with increasing axial stiffness, contrary to the uncoated specimens. This indicates that coating enhances the matrix to fibre interlocking mechanism by providing texture to the textile surface.

4.3. Comparison with the literature

Driven by the fact that textile materials have a different equivalent thickness [36] suggested to compare different TRM systems on the basis of their maximum load per unit width ratio (F_b). In, Fig. 15 a direct comparison is provided between the experimental results of the present work and the experimental results on carbon fibre textiles from the literature. The latter are collected in Table 6. For the case of the uncoated specimens examined in this work, the average value is F_b=50 kN/m, higher than the average value of the results reported in the literature (39 kN/m). In all cases, failure was due to slippage. However, the difference is well within the anticipated standard deviations for bond tests, see, also, [36] for the case of carbon fibre textiles.

For the case of the coated carbon textiles, the average value recorded in this work is 92 kN/m. This is again higher than the average F_b recorded in the literature, i.e., 76 kN/m. We note however the difference in the failure modes, i.e., textile detachment in the present work versus textile slippage in [37]. This is mainly attributed to the different mortars employed the two studies. In particular, the cement based mortar employed in [37] had a compressive and tensile strength of 17 MPa and 3.6 MPa, respectively; these were roughly 40% and 60% lower than the values of the mortar used in the present study, see also Table 2.

Overall, our experimental results agree well with the trends established in the literature for the case of carbon coated textiles and further reinforce the importance of coating vis-a-vis the exploitation of the textile. It is of interest to note, that regardless of the mesh size, the exploitation

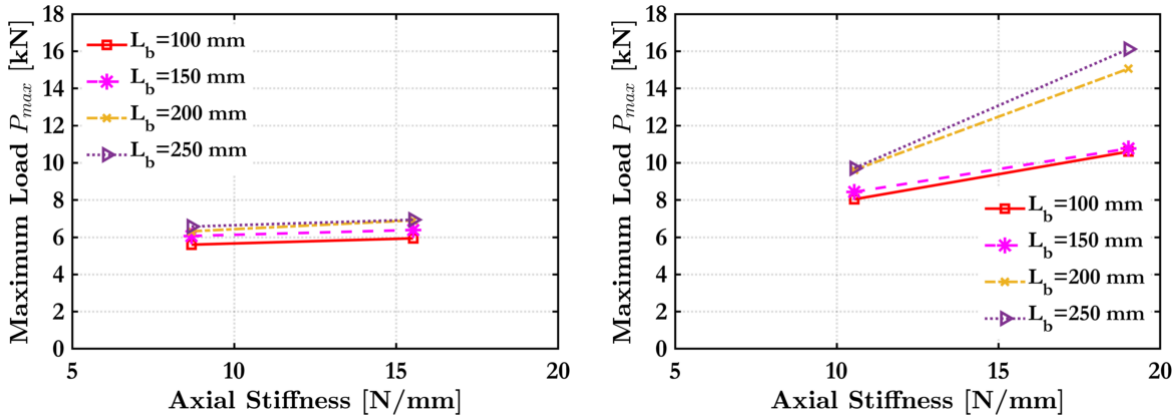

(a) Uncoated textiles (b) Coated textiles

Figure 14: Maximum load against the axial stiffness of the textile

ratios achieved at the highest bond length are within the range of 30%-40% for the uncoated specimens in all cases.

5. Analytical modelling

In this Section, the bond-slip analytical model presented in [40] is used with the objective of further verifying the two prime observations vis-a-vis the effect of the material and coating on the bond mechanism, i.e.,

- When uncoated, the interlocking mechanism is not sufficient due to the textile's flexibility. As a result the bond is primarily driven by the roving smoothness.
- When coated, the textiles are rigid enough to enable the development of the interlocking mechanism. As a result the bond is stronger in coarser mesh sizes that allow the mortar to penetrate the textile.

The analytical model is derived on the basis of the following assumptions, i.e.,

(i). The support and the lower mortar layer (Fig. 16) are assumed rigid;
(ii). the (lower and upper) mortar/reinforcement interfaces are modelled as zero-thickness elements with only shear deformability;
(iii). the upper mortar layer and the reinforcement are assumed deformable only axially.

Furthermore, the following constitutive law is assumed at interface between the textile and the lower mortar layer

$$\tau^i = \begin{cases} G^i s^i & \text{if } s^i \leq s_1 \\ 0 & \text{if otherwise} \end{cases}, \tag{3}$$

where τ^i is the shear stress at the interface, s^i is the slip at the interface, G^i is the shear modulus and s_1 is the slip threshold value.

In [40], the model is derived on the basis of appropriate equilibrium and compatibility conditions to describe the following set of individual states

(i). DP0–undamaged state;
(ii). DP1–damage involving only the interfaces (de-bonding);
(iii). DP2–damage involving only the upper mortar (cracking);
(iv). DP3–damage involving both the interfaces and the upper mortar (de-bonding/cracking).

Remark 1. *Since in our experiments the failure modes observed were textile slippage and detachment in the uncoated and coated specimens, the only relevant states are DP0 and DP1; we consider that the matrix cracking observed at the coated specimens had only a minor effect in the observed response. Furthermore, only the cases where the effective bond length has been established are examined, i.e., L_b >200 mm. Although this is not*

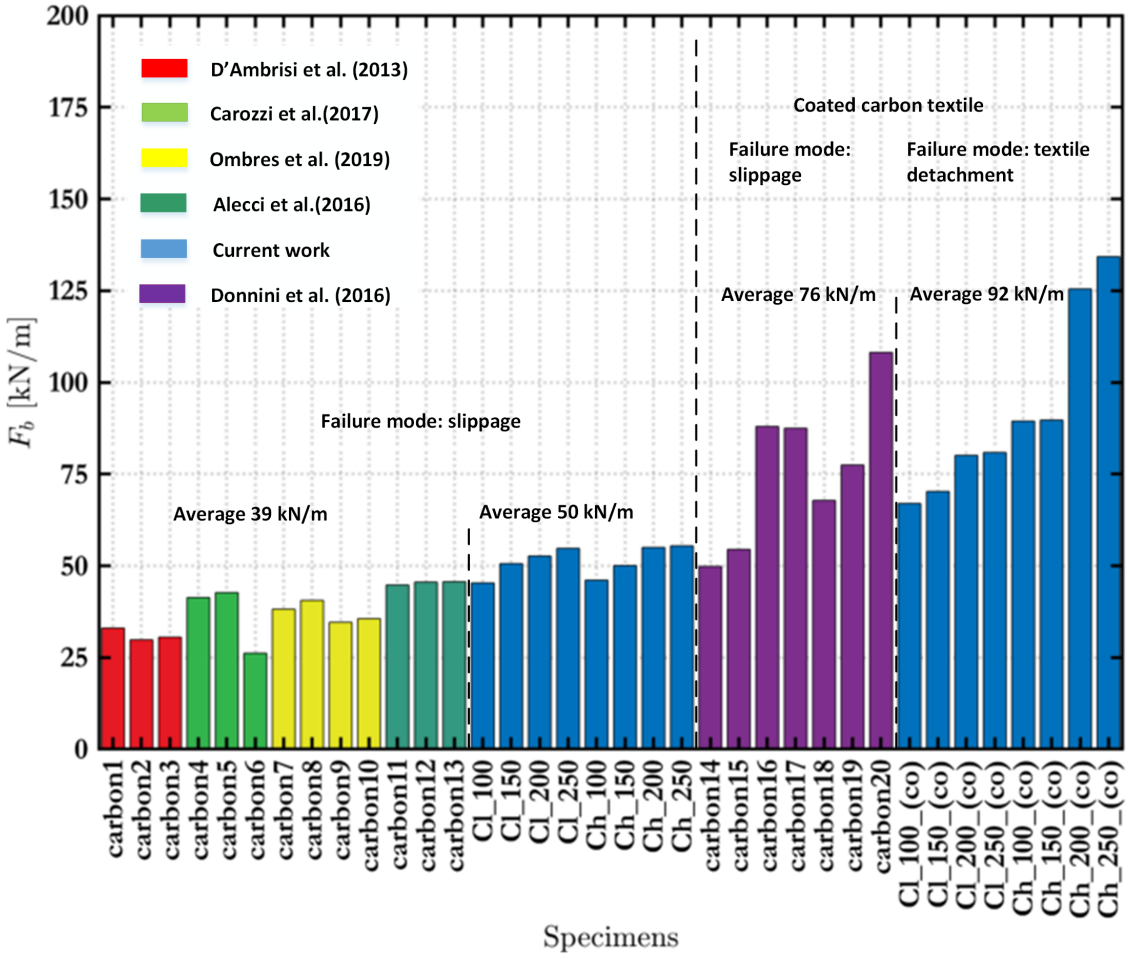

Figure 15: Carbon fiber textile reinforced mortars: Average maximum load per unit width in shear bond tests data according to Table 6

Table 6: Summary of experimental results available in the literature

Reference	Label	Textile mesh size (mm)	TRM thickness (mm)	Bond length (mm)	Width (mm)	Type of test	Maximum Load [kN]	Failure Mode	ρ_{TRM}
[19]	carbon1	10x10	NR	110	250	DF	8.26	D	-
	carbon2	10x10	NR	230	250	DF	7.46	D	-
	carbon3	10x10	NR	350	250	DF	7.64	D	-
[13]	carbon4	30x30	≈ 10	260	96	SL	3.97	D,B	0.38
	carbon5	10x10	≈ 10	260	100	SL	4.27	D,E2	0.52
	carbon6	9.4x9.4	≈ 10	260	100	SL	2.62	D	0.3
[38]	carbon7	10x10	8	150	50	SL	1.91	D	0.36
	carbon8	10x10	8	200	50	SL	2.03	D	0.38
	carbon9	10x10	8	250	50	SL	1.73	D	0.35
	carbon10	10x10	8	300	50	SL	1.78	D	0.36
[39]	carbon11	6x6	6	150	90	DF	4.03	D	0.57
	carbon12	6x6	6	200	90	DF	4.1	D	0.57
	carbon13	6x6	6	250	90	DF	4.11	D	0.57
[37]	carbon14	D20x20	10	150	60	DL	2.99	D	0.21
	carbon15	L20x20	10	150	60	DL	3.27	D	0.28
	carbon16	M20x20	10	150	60	DL	5.28	D	0.46
	carbon17	H20x20	10	150	60	DL	5.25	D,E1	0.46
	carbon18	LS20x20	10	150	60	DL	4.07	D	0.35
	carbon19	MS20x20	10	150	60	DL	4.65	D	0.40
	carbon20	HS20x20	10	150	60	DL	6.49	D,E1	0.56

DF-double-face, SL-single-lap, DL-double-lap test setup; Failure modes corresponding to Fig. 1
NR- Not Reported
ρ_{TRM}-Exploitation ratio

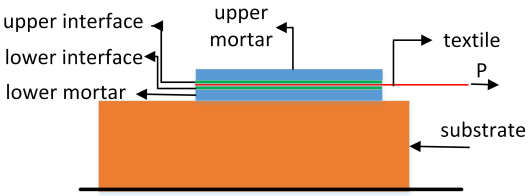

Figure 16: Schematic of the TRM system at the basis of the analytical model presented in [40].

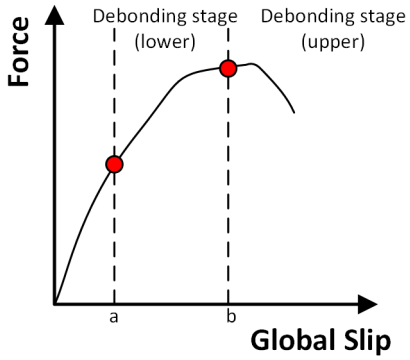

Figure 17: Debonding stages

the case for the coated heavy carbon specimens, these are still considered in the discussion for the sake of comparison.

Considering the case of a specimen subjected to a controlled displacement with a maximum value δ_{max}, the governing equations describing the response of the specimen at DP1 are defined on the basis of three steps. At the end of the first step the lower interface is assumed to attain its shear strength at the loaded end of the specimen. At the end of the second step, the upper mortar to textile interface is assumed to have reached its shear strength. At this point, the lower interface is assumed to be debonded for a length a. At the end of the final step, the global slip has assumed the value δ_{max} and the upper interface has debonded for a length b. Hence, during the entire process the specimen is assumed to be slit in parts depending on the values of the debonding lengths a and b as shown in Fig. 17.

Based on the aforementioned, the governing equations for the three sub-domains of the specimen are defined according to Eqs. (4)-(6) below. In particular, Part "1" $(0 < x < L - a - b)$ is governed by

$$\begin{cases} \dfrac{d^2 s_1^i}{dx^2} - K_1(s_1^i + s_1^e) = 0 \\ \\ (\dfrac{d^2 s_1^i}{dx^2} - \dfrac{d^2 s_1^e}{dx^2}) + K_2 s_1^e = 0 \end{cases}, \tag{4}$$

where s_1^i is the slip of the lower interface at Part "1", s_1^e is the slip of the upper interface at Part "1" and $K_1 = G^i/t_f E_f$, $K_2 = G^i/t_c E_c$ are material constants; t_c and E_c are the thickness of the upper mortar layer and the mortar Young's modulus, respectively.

Similarly, Part "2" $(L - a - b < x < L - b)$ is governed by

$$\begin{cases} \dfrac{d^2 s_1^i}{dx^2} - K_1 s_1^e = 0 \\ \\ (\dfrac{d^2 s_1^i}{dx^2} - \dfrac{d^2 s_1^e}{dx^2}) + K_2 s_1^e = 0 \end{cases} \tag{5}$$

and finally Part "3" (L-b< x< L) is governed by

$$\begin{cases} \dfrac{d^2 s_3^i}{dx^2} = 0 \\ \\ \dfrac{d^2 s_3^i}{dx^2} - \dfrac{d^2 s_3^e}{dx^2} = 0 \end{cases} \tag{6}$$

Eqs. (4)-(6) can be solved considering also the appropriate boundary and continuity conditions. Further information along with a thorough discussion on the application of the model can be found in [40], see, also, [16].

In the following, the procedure for identifying the interface properties to be used in the analytical model is described. In all cases, the textile Young's modulus E_f is set according to the tensile tests results shown in Table 4. The mortar's Young's modulus is set to E_c=15000 MPa according to the manufacturer data sheets. The upper layer mortar thickness is set to t =4 mm and the textile thickness according to Table 5. The shear strength of the interface τ_i and the corresponding slip s_1 is inferred from the experimental results as discussed in Sections 5.1 and 5.2 for the coated and uncoated specimens, respectively. The values of all material parameters are summarized in Table 7.

Table 7: Material parameters employed in the analytical model. The identified parameters are highlighted in grey color.

Material	E_f	E_c*	t	t_f	τ_i	s_1
[-]	[GPa]	[MPa]	[mm]	[mm]	[MPa]	[mm]
Light carbon	140	15000	4	0.062	0.33	1.3
Heavy carbon	160	15000	4	0.097	0.33	0.9
Coated light carbon	170	15000	4	0.062	0.6	1.4
Coated heavy carbon	196	15000	4	0.097	0.75	1.75
*Data reported in the data sheet						

5.1. Coated specimens

In the case of the coated specimens, the failure mode was due to detachment. We use the force slip response of the heavy carbon coated specimen with L_b=250 mm and determine the corresponding interfacial shear strength

$$\tau_i^{Ch\_co} = 0.75 \text{ MPa}.$$

The corresponding slip s_1 is measured from the plot and found equal to $s_1 = 1.75$ mm. These parameters are then used to generate the analytical force slip response of the coated carbon specimen at L_b=200 mm. The resulting analytical versus the experimental force-slip plots are shown in Fig. 18.

Next, the interfacial shear strenth of the light carbon coated specimens is directly estimated through the following equation

$$\tau_i^{Cl\_co} = \alpha \tau_i^{Ch\_co}, \tag{7}$$

where α is the ratio of the light to heavy carbon mesh size, i.e.,

$$\alpha = 0.8$$

The resulting shear strength is $\tau_i^{Cl\_co} = 0.6$ MPa. The corresponding slip is measured from the plot and found equal to $s_1 = 1.40$ mm. The resulting force slip plots for the light carbon coated textile specimens are shown in Fig. 19. Despite the fact that the interface shear strength of the light carbon specimens was inferred using Eq. (7), the analytical model practically matches the experimental response for the case of L_b=200 mm. In the case of L_b=250 mm, the predicted maximum load is 1.5% higher than the experimentally measured one. This fact reinforces our observation that coating renders the textile adequately rigid so that the mesh size becomes relevant in the bond transfer mechanism.

5.2. Uncoated specimens

In the uncoated specimens, the failure mode was due to textile slippage within the matrix. Here, Ch_250 specimen is used to identify the shear strength of the interface. The identified value is t_i=0.33 MPa. This value is then retained constant for all heavy and light uncoated specimens. The corresponding value of the slip is s_1=1.3 mm for the heavy carbon specimens and s_1=0.9 mm for the light carbon specimens. The resulting plots are shown in Fig. 20.

In all cases, the fit between the analytical prediction and the experimental results is acceptable. The highest discrepancy in terms of maximum load is observed in the case of specimen Cl_250 where the analytical prediction is 4.5% higher than the experimental one. Once again, this reaffirms our observation that in the case of the uncoated specimens the bond mechanism is driven by the smoothness of the roving surface and the chemistry of the bond rather than the geometry of the textile mesh.

As a means of further verification, we use the analytical model to predict the maximum load on the uncoated specimens (carbon1-12) reported in Table 6. In all cases, the predictions are established using a value of t_i=0.33 MPa. The remaining pertinent parameters, i.e., bonded length, specimen width, the mortar and the textile properties are set to their corresponding values found in the literature. The predicted maximum load for each case is compared to the average experimental load in Fig. 21.

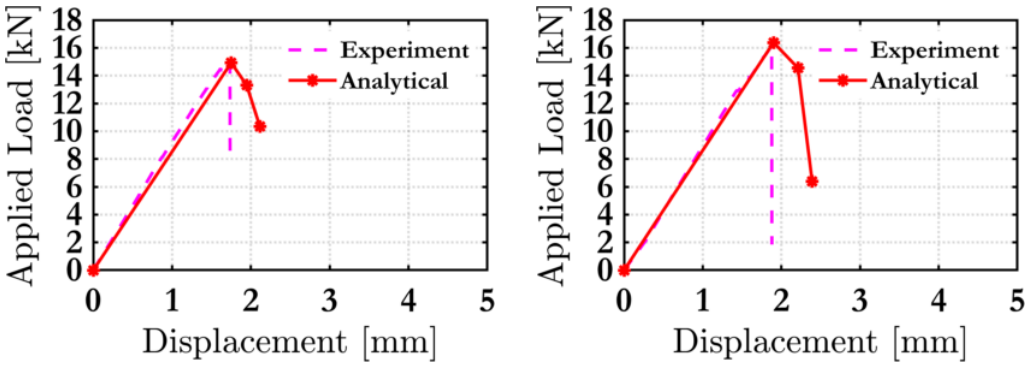

Figure 18: Analytical predictions versus experimental measurements for the heavy carbon coated textile fibre specimens (a) L_b =200 mm (b) L_b =250 mm

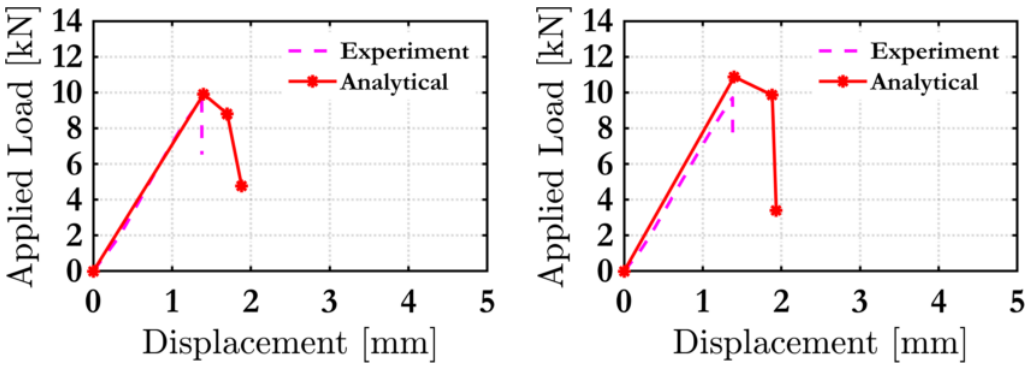

Figure 19: Analytical predictions versus experimental measurements for the light carbon coated textile fibre specimens (a) L_b =200 mm (b) L_b =250 mm

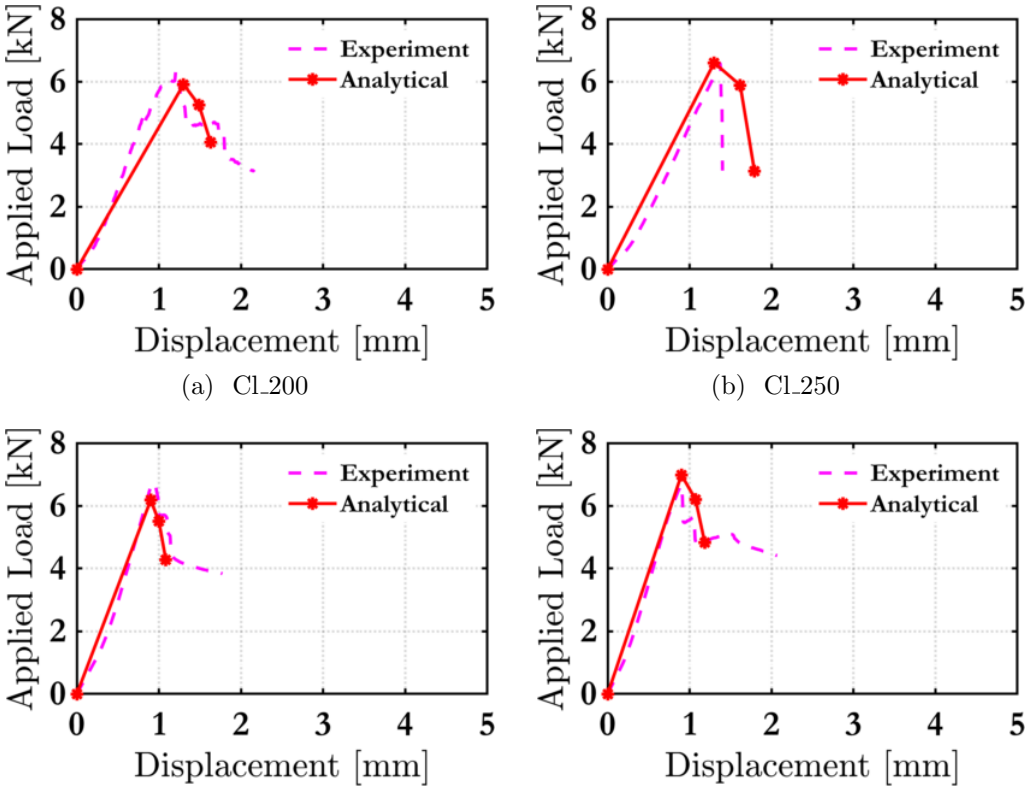

Figure 20: Uncoated fibre textile specimens: Analytical predictions versus experimental measurements

In most cases, a very good agreement is observed. The highest discrepancy between the experimental results and analytical prediction occurs for experiment 6. In this case, the predicted maximum load is 60% higher than the the experimental one. Given that the mesh geometry, the mechanical properties, and the bond length were practically identical, we believe that this difference could be potentially attributed to the different mortar mixes implemented in the two studies and hence the differences in the corresponding mechanical properties and also to the chemistry of the bond.

6. Conclusions

An extensive experimental campaign was conducted to investigate the TRM to masonry bond strength considering as key investigated parameters the bond length, the textile fibre material, the effect of epoxy resin coating, and the strength of the mortar matrix. The main conclusions drawn

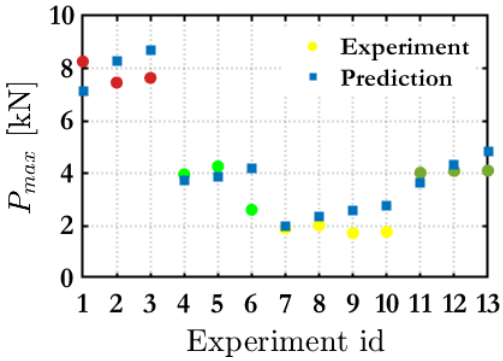

Figure 21: Comparisons between the analytical predictions and the bond tests on the uncoated textiles reported in Table 6. Color coding corresponds to Fig. 15

for the experiments are summarised below:

(i) By increasing the bond length, the bond capacity increased bi-linearly for all materials examined. After a certain bond length, i.e., the effective bond length L_{eff}, the bond capacity increased marginally. With the exception of the coated heavy carbons, the bond length was found to be L_{eff} =200-250 mm. The experimental results are inconclusive for the case of the heavy carbon coated specimens.

(ii) The in-house epoxy resin coating positively effected the maximum load capacity in all bond lengths. The coated light and heavy carbon demonstrated increased values of the maximum load by 42%, and 132%, respectively when compared with their uncoated counterparts (250 mm bond length case).

(iii) When coated, the light and heavy carbon fibre textiles demonstrated identical exploitation ratios for the same bond length. This indicates that the light carbon fibre textile is a more viable solution of strengthening due to its lower costs.

(iv) Increasing values of the maximum load are associated with the increasing axial stiffness of the textile only in the case of the coated specimens. Coating renders the textile stiffer hence preventing distortions within the matrix. This allows for a uniform stress distribution in the textile eventually enabling it to develop higher stresses.

(v) Coating further magnified the effect of the bond length. For the same bond length, the coated specimens demonstrate significantly higher values of maximum load compared to their uncoated counterparts. This indicates that the matrix to fibre interface properties are enhanced due to the surface roughness provided by the coating.

(vi) Analytical predictions, on the basis of rational assumptions, highlight that in the case of uncoated carbon fibre textiles, the bond strength is regulated by the surface properties of the fibre rather than the geometry of the textile mesh.

Acknowledgement

The first author would like to acknowledge the financial support of the JSC Center for International Programs - Bolashak Ministry of education Republic of Kazakhstan. The second author would like to acknowledge the support of the Marie Sklodowska-Curie Individual Fellowship grant "AI2AM: Artificial Intelligence driven topology optimisation of Additively Manufactured Composite Components", No. 101021629.

References

[1] C. Papanicolaou, T. Triantafillou, M. Lekka, Externally bonded grids as strengthening and seismic retrofitting materials of masonry panels, Construction and Building Materials 25 (2011) 504–514.

[2] E. Bernat, L. Gil, P. Roca, C. Escrig, Experimental and analytical study of trm strengthened brickwork walls under eccentric compressive loading, Construction and Building Materials 44 (2013) 35–47.

[3] M. Shabdin, M. Zargaran, N. K. Attari, Experimental diagonal tension (shear) test of un-reinforced masonry (URM) walls strengthened with textile reinforced mortar (TRM), Construction and Building Materials 164 (2018) 704–715.

[4] P. D. Askouni, C. G. Papanicolaou, Experimental investigation of bond between glass textile reinforced mortar overlays and masonry: the effect of bond length, Materials and Structures/Materiaux et Constructions 50 (2017). doi:10.1617/s11527-017-1033-7.

[5] C. G. Papanicolaou, T. C. Triantafillou, K. Karlos, M. Papathanasiou, Textile-reinforced mortar (TRM) versus FRP as strengthening material of URM walls: in-plane cyclic loading, Materials and structures 40 (2007) 1081–1097.

[6] C. G. Papanicolaou, T. C. Triantafillou, M. Papathanasiou, K. Karlos, Textile reinforced mortar (TRM) versus FRP as strengthening material of URM walls: out-of-plane cyclic loading, Materials and structures 41 (2008) 143–157.

[7] M. Harajli, H. ElKhatib, J. T. San-Jose, Static and Cyclic Out-of-Plane Response of Masonry Walls Strengthened Using Textile-Mortar System, Journal of Materials in Civil Engineering 22 (2010) 1171–1180. doi:10.1061/(ASCE)MT.1943-5533.0000128.

[8] L. Garmendia, I. Marcos, E. Garbin, M. R. Valluzzi, Strengthening of masonry arches with textile-reinforced mortar: experimental behaviour and analytical approaches, Materials and structures 47 (2014) 2067–2080.

[9] T. Triantafillou, Strengthening of existing masonry structures: Concepts and structural behavior, in: T. Triantafillou (Ed.), Textile Fibre Composites in

Civil Engineering, Woodhead Publishing, 2016, pp. 361–374. doi:https://doi.org/10.1016/B978-1-78242-446-8.00016-1.

[10] L. A. S. Kouris, T. C. Triantafillou, State-of-the-art on strengthening of masonry structures with textile reinforced mortar (TRM), Construction and Building Materials 188 (2018) 1221–1233. URL: https://doi.org/10.1016/j.conbuildmat.2018.08.039. doi:10.1016/j.conbuildmat.2018.08.039.

[11] G. de Felice, M. A. Aiello, C. Caggegi, F. Ceroni, S. De Santis, E. Garbin, N. Gattesco, Ł. Hojdys, P. Krajewski, A. Kwiecień, M. Leone, G. P. Lignola, C. Mazzotti, D. Oliveira, C. Papanicolaou, C. Poggi, T. Triantafillou, M. R. Valluzzi, A. Viskovic, Recommendation of RILEM Technical Committee 250-CSM: Test method for Textile Reinforced Mortar to substrate bond characterization, Materials and Structures/Materiaux et Constructions 51 (2018) 1–9. doi:10.1617/s11527-018-1216-x.

[12] M. Leone, M. A. Aiello, A. Balsamo, F. G. Carozzi, F. Ceroni, M. Corradi, M. Gams, E. Garbin, N. Gattesco, P. Krajewski, et al., Glass fabric reinforced cementitious matrix: Tensile properties and bond performance on masonry substrate, Composites Part B: Engineering 127 (2017) 196–214.

[13] F. G. Carozzi, A. Bellini, T. D'Antino, G. de Felice, F. Focacci, Ł. Hojdys, L. Laghi, E. Lanoye, F. Micelli, M. Panizza, C. Poggi, Experimental investigation of tensile and bond properties of Carbon-FRCM composites for strengthening masonry elements, Composites Part B: Engineering 128 (2017) 100–119. doi:10.1016/j.compositesb.2017.06.018.

[14] B. Ghiassi, D. V. Oliveira, V. Marques, E. Soares, H. Maljaee, Multi-level characterization of steel reinforced mortars for strengthening of masonry structures, Materials and Design 110 (2016) 903–913. doi:10.1016/j.matdes.2016.08.034.

[15] L. Ascione, G. De Felice, S. De Santis, A qualification method for externally bonded Fibre Reinforced Cementitious Matrix (FRCM) strengthening systems, Composites Part B: Engineering 78 (2015) 497–506. doi:10.1016/j.compositesb.2015.03.079.

[16] X. Wang, C. C. Lam, V. P. Iu, Bond behaviour of steel-TRM composites for strengthening masonry elements: Experimental testing and numerical modelling, Construction and Building Materials 253 (2020) 119157.

[17] G. De Felice, S. De Santis, L. Garmendia, B. Ghiassi, P. Larrinaga, P. B. Lourenço, D. V. Oliveira, F. Paolacci, C. G. Papanicolaou, Mortar-based systems for externally bonded strengthening of masonry, Materials and structures 47 (2014) 2021–2037.

[18] P. D. Askouni, C. C. G. Papanicolaou, Comparison of double-lap/double-prism and single-lap/single-prism shear tests for the trm-to-masonry bond assessment, in: V. Mechtcherine, V. Slowik, P. Kabele (Eds.), Strain-Hardening Cement-Based Composites, Springer Netherlands, Dordrecht, 2018, pp. 527–534.

[19] A. D'Ambrisi, L. Feo, F. Focacci, Experimental and analytical investigation on bond between Carbon-FRCM materials and masonry, Composites Part B: Engineering 46 (2013) 15–20. doi:10.1016/j.compositesb.2012.10.018.

[20] F. G. Carozzi, C. Poggi, Mechanical properties and debonding strength of Fabric Reinforced Cementitious Matrix (FRCM) systems for masonry strengthening, Composites Part B: Engineering 70 (2015) 215–230. doi:10.1016/j.compositesb.2014.10.056.

[21] L. Ombres, N. Mancuso, S. Mazzuca, S. Verre, Bond between carbon fabric-reinforced cementitious matrix and masonry substrate, Journal of Materials in Civil Engineering 31 (2018) 04018356.

[22] G. P. Lignola, C. Caggegi, F. Ceroni, S. De Santis, P. Krajewski, P. B. Lourenço, M. Morganti, C. C. Papanicolaou, C. Pellegrino, A. Prota, L. Zuccarino, Performance assessment of basalt FRCM for retrofit applications on masonry, Composites Part B: Engineering 128 (2017) 1–18. doi:10.1016/j.compositesb.2017.05.003.

[23] S. Barducci, V. Alecci, M. De Stefano, G. Misseri, L. Rovero, G. Stipo, Experimental and analytical investigations on bond behavior of Basalt-FRCM systems, Journal of Composites for Construction 24 (2019) 04019055.

[24] S. R. Maroudas, C. C. G. Papanicolaou, Effect of high temperatures on the trm-to-masonry bond, in: 1 (Ed.), Mechanics of Masonry Structures Strengthened with Composite Materials II, volume 747 of *Key Engineering Materials*, Trans Tech Publications Ltd, 1, 2017, pp. 533–541. doi:10.4028/www.scientific.net/KEM.747.533.

[25] Luciano Ombres, Antonio Iorfida, Stefania Mazzucaa, Salvatore Verreço, Bond analysis of thermally conditioned FRCM-masonry joints, Measurement 125 (2018) 509–515.

[26] P. D. Askouni, C. G. Papanicolaou, Experimental investigation of bond between glass textile reinforced mortar overlays and masonry: the effect of bond length, Materials and Structures 50 (2017) 164.

[27] A. d. A. Vieira, S. Triantafyllou, D. Bournas, Strengthening of rc frame subassemblies against progressive collapse using trm and nsm reinforcement, Engineering Structures 207 (2020) 110002.

[28] F. Kariou, S. P. Triantafyllou, D. Bournas, L. Koutas, Out-of-plane response of masonry walls strengthened using textile-mortar system, Construction and Building Materials 165 (2018) 769–781.

[29] F. A. Kariou, S. P. Triantafyllou, D. A. Bournas, Trm strengthening of masonry arches: An experimental investigation on the effect of strengthening layout and textile fibre material, Composites Part B: Engineering 173 (2019) 106765.

[30] G. de Felice, M. A. Aiello, A. Bellini, F. Ceroni, S. De Santis, E. Garbin, M. Leone, G. P. Lignola, M. Malena, C. Mazzotti, M. Panizza, M. R. Valluzzi, Experimental characterization of composite-to-brick masonry shear bond, Materials and Structures/Materiaux et Constructions 49 (2016) 2581–2596. doi:10.1617/s11527-015-0669-4.

[31] B. EN, 772-1.(2011), Methods of test for masonry units (2011).

[32] B. EN, 1015-11: Methods of test for mortar for masonry–part 11: Determination of flexural and compressive strength of hardened mortar, European Committee for Standardization, Brussels (1999).

[33] D. ASTM, Standard test method for breaking strength and elongation of textile fabrics (grab test), Current edition approved (1995) 674–681.

[34] S. M. Raoof, L. N. Koutas, D. A. Bournas, Textile-reinforced mortar (TRM) versus fibre-reinforced polymers (FRP) in flexural strengthening of RC beams, Construction and Building Materials 151 (2017) 279–291.

[35] S. De Santis, G. de Felice, Steel reinforced grout systems for the strengthening of masonry structures, Composite Structures 134 (2015) 533–548.

[36] G. de Felice, T. D'Antino, S. De Santis, P. Meriggi, F. Roscini, Lessons learned on the tensile and bond behavior of fabric reinforced cementitious matrix (FRCM) composites, Frontiers in Built Environment 6 (2020) 5.

[37] J. Donnini, V. Corinaldesi, A. Nanni, Mechanical properties of frcm using carbon fabrics with different coating treatments, Composites Part B: Engineering 88 (2016) 220–228.

[38] L. Ombres, N. Mancuso, S. Mazzuca, S. Verre, Bond between carbon fabric-reinforced cementitious matrix and masonry substrate, Journal of Materials in Civil Engineering 31 (2018) 04018356.

[39] V. Alecci, M. De Stefano, R. Luciano, L. Rovero, G. Stipo, Experimental investigation on bond behavior of cement-matrix–based composites for strengthening of masonry structures, Journal of Composites for Construction 20 (2015) 04015041.

[40] E. Grande, M. Imbimbo, E. Sacco, Numerical investigation on the bond behavior of FRCM strengthening systems, Composites Part B: Engineering 145 (2018) 240–251.